Decoding of standard and non-standard visuomotor associations from parietal cortex

Published Version:
Filippini M., Morris A.P., Breveglieri R., Hadjidimitrakis K., Fattori P. (2020). Decoding of standard and non-standard visuomotor associations from parietal cortex. JOURNAL OF NEURAL ENGINEERING, 17(4), 1-15 [10.1088/1741-2552/aba87e].

Availability:
This version is available at: https://hdl.handle.net/11585/789028 since: 2021-01-16

Published:
DOI: http://doi.org/10.1088/1741-2552/aba87e

(Article begins on next page)

Journal of Neural Engineering

Decoding of standard and non-standard visuomotor associations from parietal cortex.

To cite this article before publication: Matteo Filippini *et al* 2020 *J. Neural Eng.* in press https://doi.org/10.1088/1741-2552/aba87e

Decoding of standard and non-standard visuomotor associations from parietal cortex.

M. FILIPPINI[12], A.P. MORRIS[3], R. BREVEGLIERI[1], K. HADJIDIMITRAKIS[1,3*], P. FATTORI[12*];

[1]University of Bologna, Department of Biomedical and Neuromotor Sciences, Bologna, Italy;

[2] ALMA-AI: Alma Mater Research Institute for Human-Centered Artificial Intelligence

[3]Neuroscience Program, Biomedicine Discovery Institute, Department of Physiology, Monash University, Clayton, Australia

[*] Equal senior authors

Correspondence: Dr. Matteo Filippini, Ph.D,

Department of Biomedical and Neuromotor Sciences,

University of Bologna, Piazza di Porta San Donato 2,

Bologna 40126, Italy E-mail: matteo.filippini7@unibo.it

Abstract

Objective

Neural signals can be decoded and used to move neural prostheses with the purpose of restoring motor function in patients with mobility impairments. Such patients typically have intact eye movement control and visual function, suggesting that cortical visuospatial signals could be used to guide external devices. Neurons in parietal cortex mediate sensory-motor transformations, encode the spatial coordinates for reaching goals, hand position and movements, and other spatial variables. We studied how spatial information is represented at the population level, and the possibility to decode not only the position of visual targets and the plans to reach them, but also conditional, non-spatial motor responses.

Approach

The animals first fixated one of nine targets in 3D space and then, after the target changed color, either reached toward it, or performed a non-spatial motor response (lift hand from a button). Spiking activity of parietal neurons was recorded in monkeys during two tasks. We then decoded different task related parameters.

Main results

We first show that a maximum-likelihood estimation (MLE) algorithm trained separately in each task transformed neural activity into accurate metric predictions of target location. Furthermore, by combining MLE with a Naïve Bayes classifier, we decoded the monkey's motor intention (reach or hand lift) and the different phases of the tasks. These results show that, although V6A encodes the spatial location of a target during a delay period, the signals they carry are updated around the movement execution in an intention/motor specific way.

Significance

These findings show the presence of multiple levels of information in parietal cortex that could be decoded and used in brain machine interfaces to control both goal-directed movements and more cognitive visuomotor associations.

Keywords

Reaching, brain computer interfaces, decoding, electrophysiology, posterior parietal cortex, monkey

1. Introduction

A large body of evidence shows that motor intentions can be decoded from neural activity and used to control artificial limbs (1–6). In most of these cases, neural activity was recorded from motor cortex, where signals are highly correlated with desired movement trajectories (1,3). An alternative approach is to exploit signals earlier in the sensorimotor pathways, particularly in posterior parietal cortex (PPC), where neurons are sensitive to movement parameters and more abstract representations of intention and visuospatial attention (7–13). The spatial target of a reach, for example, can be decoded from a small number of neurons in PPC in monkeys (14–17), and from fMRI signals (18,19) or intracortical signals (2) in humans.

A device that relies on signals from PPC, rather than from motor cortex, has the potential advantage that it could (also) infer the intended outcome of an action rather than the kinematics of a specific movement. This could provide greater flexibility in its use across a range of assistive technologies. However, PPC signals are multi-modal and high-dimensional (8,20,21), making difficult to disentangle between these signals.

Here, we tested whether multiple task- and intention-related variables could be decoded simultaneously from population activity in area V6A, located in the posterior parietal cortex (PPC) (22,23). V6A neurons are involved in both reaching and grasping (24–27), and are tuned for kinematic parameters such as direction (28,29) and amplitude of hand movement (24). In addition, they encode visual target location in 3D in the absence of reaching (27,30–32), thus enabling the use of visuospatial information in task contexts where no arm movement is planned.

To test this hypothesis, we decoded neural activity recorded from area V6A in macaques while they performed sequentially two sensorimotor tasks (Fig. 1). Both tasks required fixation of a visual target that varied position in 3D space across trials, but they differed in the type of motor response required: a reach movement towards the target (fixate-to-reach task), or a non-spatial motor response (fixate-to-hand lift task) that was instructed by the color code of the target, but not directed towards it. We used a Maximum Likelihood Estimator (MLE) that permits a metric estimation of the target position.

We then compared population codes between the two tasks during the delay period. At the single neuron level, we recently reported that the most represented type of V6A cells (44%) showed different firing between these two tasks (33), so we expected that the population signals would be different. In addition, we looked for activity patterns related to distinct task stages and how they gradually evolved to support the movement. These switches can be useful to trigger prosthesis movement (17,34).

We found that we could reliably decode: target position, type of intended movement and different cognitive states from the very same population of neurons. At the same time, generalization analysis across tasks showed that the neural codes were very similar in most task phases and diverged only immediately before the movement onset. The finding that multiple variables and types of motor responses were coded dynamically in the same brain area could be exploited for neuroprosthetic applications.

2. **Methods**

The experimental part of this study was performed in accordance with the guidelines of the EU Directives (86/609/EEC; 2010/63/EU) and the Italian national law (D.L. 116-92, D.L. 26-2014) on the use of animals in scientific research. Protocols were approved by the Animal-Welfare Body of the University of Bologna. During training and recording sessions, particular attention was paid to any behavioral and clinical sign of pain or distress.

2.1 Experimental Procedures

Two male macaque monkeys (Macaca fascicularis) weighing 4.4 kg (Monkey 1, M1) and 3.8 kg (Monkey 2, M2) were used. Single cell activity was recorded extracellularly by means of single electrode from the anterior bank of the parieto-occipital sulcus (POs). We performed multiple electrode penetrations using a five-channel multielectrode recording system that permitted to record from up to five single electrodes at once (Thomas Recording GmbH, Giessen, Germany). We recorded the activity of 162 V6A (36) neurons, 100 cells from M1 and 62 cells from M2. Although five electrodes was the maximum number of our recording system, on average we were recording from 2-3 neurons at once; in total, the number of sessions distributed between M1 and M2 was 45 (22 + 23). Action potentials (spikes) in each channel were isolated with a waveform discriminator (Multi Spike Detector; Alpha Omega Engineering Nazareth, Israel) and were sampled at 100 kHz. Quality of single-unit isolation was determined by the homogeneity of spike wave forms and clear refractory periods in ISI histograms during spike-sorting. Only well-isolated units not changing across tasks were considered. The experimental procedures are described in full detail in Breveglieri et al. (2014).

2.2 Behavioral Tasks

Electrophysiological signals were collected while the monkeys were performing two instructed-delay tasks: a fixate-to-reach task (fix-reach) and a fixate-to-lift hand task (fix-lift), as illustrated in Figure 1. In both tasks, one of nine targets placed in several locations in 3-D space was switched on and the animal had to fixate it and, when instructed (target color change), either perform a reach toward the target (fix-reach), or lift the hand from the home button (fix-lift). Monkeys sat in a primate chair, with the head restrained, and faced a horizontal panel located at eye level. Nine light-emitting diodes (LEDs) mounted on the panel at different distances from the eyes were used as fixation and reaching targets (Figure 1A, left). As shown in the right part of Figure 1A, the nine target LEDs were arranged in a radial grid consisting of three directions: version angles of −15°, 0°, and +15° and three depths i.e., vergence angles of 17.1°, 11.4°, and 6.9°. The two animals had the same interocular distance (3.0 cm), so we placed the grid at the same distance from the monkeys in both animals (nearest targets: 10 cm; intermediate targets: 15 cm; far targets: 25 cm). The range of vergence angles was chosen to be within the limits of peripersonal space, so the monkeys were able to reach all target positions. The animals performed the tasks with the arm contralateral to the recording site. The two tasks were performed in separate blocks. In case of fix-lift task, a plexiglass barrier prevented the hand movement toward the target.

In both tasks, the animal initiated a trial by pressing and holding a home button (HB; 2.5 cm in diameter, Figure 2A) placed 5 cm in front of the torso, outside the field of view (FREE epoch). After a delay of 1000 ms, one of the nine LEDs was turned on in green, cuing the animal to initiate fixation. After a delay of 1700–2500 ms (DELAY epoch), the LED changed to red, cuing the animal to either perform a reach to the target (fix-reach task) or to simply release the button (fix-lift task) (MOV epoch). In the case of fix-reach task, monkeys had 1 sec after the go signal to reach the target, otherwise the trial was aborted. Then, monkeys pressed the target and held the hand on it for 800–1200 ms. The target offset cued the monkeys to release the LED and return to the home button, which ended the trial and allowed monkeys to receive reward. In the case of fix-lift task, monkeys had 1 s to release the button to have the reward.

Only correctly executed trials were used in this analysis. We collected 10 correct trials for each of the 9 conditions (targets) and for each tested task.

2.3 Data Analysis

2.3.1 Preprocessing. Neurons activities were analyzed as spike counts within single trials. The spike times on each trial were counted within a 100-ms window that stepped in 100 ms increments. Because these neurons were not recorded simultaneously, a “trial” in this context refers to a synthetic dataset in which a single experimental trial was drawn randomly for each neuron from a common behavioral condition and collated. This is a common and useful way to simulate population codes in the brain from single neuron data (37–40). It should be noted, however, that this approach ignores potential effects of correlated spike-count variability on the coding of target position.

2.3.2 Population Decoding. To decode the different parameters which describes the fix-reach or the fix-lift task, two different decoding algorithms were used in our analysis: a Maximum Likelihood Estimator (MLE) and a Naïve Bayes classifier (NB). Metric estimation of target positions (in a 2D grid) relied on MLE decoding algorithm. This algorithm was used successfully to decode eye position signals from macaque parietal and temporal cortex (37,38). We adapted this implementation to our motor task using signals from area V6A. In addition to the decoding of the target spatial position, we examined two additional parameters: given a random bin of activity, whether it was possible to predict the current task type (fix-reach or fix-lift) and the current task phase (epoch free, or delay, or movement, see below). These latter parameters, together with metric estimation of target location provide a detailed snapshot of the ongoing action. In particular, we combined the MLE and NB decoders to recognize whether the monkey performed a reach toward the target or simply lifted his hand off the button. Decoding of task phase was performed using a simple NB implementation to identify the different epochs of tasks.

2.3.3 Target decoding. MLE decoder estimated the spatial coordinates of targets given the population neural activity. The implementation is described in full detail in Morris et al. (37,38): here are summarized the key steps. A regression surface (second order polynomial, eq.1 and a real example in Fig.2A) was calculated for each neuron and it was used to estimate the effect of target position (*direction X, depth Y*) on mean spike counts ($\hat{c}$).

Eq. 1 $$\hat{c}(X,Y) = a_0 + a_1X + a_2Y + a_3X^2 + a_4Y^2 + a_5XY$$

Assuming Poisson statistics, eq.1 becomes a description of how both the mean and variance (both equal to λ) of spike counts varied as a function of target position. Thus, conditional probability over spike counts for a given target position (*x,y*) was:

Eq. 2 $$\hat{p}(C|x,y) = Poisson[\lambda(\mathrm{x},\mathrm{y})] \text{ where } \lambda(\mathrm{x},\mathrm{y}) = \hat{c}(x,y)$$

Equation 2 provides a critical quantitative link between target position and the neural response: the probability of a neural response given a target position (in statistical terms, a “likelihood function”); but without additional steps, they do not provide the information needed for decoding. Decoding implements the reverse direction of inference, so it requires an estimate of the probability of each target position given an observed spike count (i.e. $p(X,Y|c)$, the posterior probability distribution (Fig. 2B). These two types of conditional probability are related via the Bayes rule. Assuming statistical independence among N neurons, the optimal way to combine posterior probability density functions across the population is to take their product, which is usually implemented as a sum of their logarithms. As the final step, the eye position associated with the maximum a posteriori (MAP) log-likelihood (i.e., the MAP estimate) in log $p(X,Y|C\ population)$ was selected as the point estimate for target direction and depth (Fig. 2C). To assess the ability of our model to predict the correct target positions, we used a R^2 metric, R^2 is the proportion of the variance in the dependent variable (*x,y* of targets) that is predictable from the independent variable (decoded spike counts). Accuracy was evaluated as the Euclidean distance from the mean of predictions (over cross-validation) to the real target position. Similarly, precision was computed as distance from predictions to the mean of predictions for a given target position.

2.3.4. Task type decoding. To identify which task the monkey executed, i.e. fix-reach or fix-lift, we used a combination of the MLE decoder used for target decoding and a Bayesian classifier. In this case we were not interested to predict the target position, so the analysis was conducted pooling together spike counts from different positions but keeping separate the data of the two tasks. First, a regression surface for each neuron was calculated in the same way as the method proposed above. Second, residuals from surface fitting were used to train a NB classifier to discriminate between tasks. Residuals are a common way to express the distance between the model resulting from the fitting and the real data. Deviations from the model can be used as feature for machine learning algorithms, in the way that they are very informative about the uncommon part between the two datasets. Since we wanted to solve a simple binary classification problem between two classes (i.e. given the spike count of any bin taken in the interval of one of the two tasks predict which task it belonged to) we adopted a Naïve Bayesian classifier. Keeping the assumption of independence between features, Naive Bayesian classifiers are robust, fast and widely used as neural decoders in case the goal is to classify discrete quantities as neural states can be. Matlab *'ClassificationNaiveBayes'* class implementation was used. Results are given as recognition rate computed from a 50-fold cross-validation. Such cross-validation was used to keep the analysis fair compared to the others where fewer trials were available; here 90 trials per class were available and keeping out 3 trials for testing per cross-validation iteration seemed a good compromise.

2.3.5. Task phase decoding. To test whether the spike counts (100ms bin) contained information about the different task phases, we trained a NB classifier to discriminate between the three FREE, DELAY and MOVEMENT states (see 2.2 for behavioral epochs). Simple spike counts were used to build-up the population feature vectors with dimension n neurons by 10 trials x 9 conditions x 3 states (270 vectors). The three states correspond to three classes for the classifier. A leave one out cross-validation over 10 trials was used. A custom Python script based on *scikit-learn* implementation of Naïve Bayes classifier with a Poisson assumption was used (41). Results are reported as probability for each state along the time (Fig. 7A) and confusion matrices (Fig. 7B).

2.3.6 Cross-validation. Leave-One-Out (LOO) cross-validation was used to ensure that the results of population decoding reflected reliable characteristics of the neural code for target position and not effects of overfitting. For each cross-validation set, the spike counts at each of the 9 target positions and the associated regression coefficients were estimated from 90% of the available trials for each neuron ("training set"). Decoding was then performed on 100 synthetic trials (see 2.3.1) drawn at random from the remaining trial for each neuron. Unless otherwise stated, the population decoding results presented herein were therefore derived from 900 synthetic trials (100 test trials for each cross-validation sets).

2.3.7 Generalization. In order to compare neural activation patterns under different experimental paradigm we can build models (training the algorithm) on neural data from a specific task, then using data from the other task to make predictions. Prediction accuracy (expected vs predicted) represents metric for the grade of similarity between codes. Given the example for training on fix-reach and testing on fix-lift task, we computed the regression surfaces with spike counts from fix-reach task.

3. Results

Two monkeys were trained to perform in randomized block sequence the fix-reach and the fix-lift task. Fixation and reach targets were nine touch-sensitive LEDs, placed in the 3-D space at three different directions (version angles -15°, 0°, +15°) and three different distances (vergence angles, 17.1°, 11.4° and 6.9°; Fig. 1A). The two tasks were identical except for the motor response (reaches vs. hand lifts; Fig.1B-C). Neurons were recorded from two macaque monkeys (see 2.1 for more details) and were included in the subsequent analyses, only if ten trials were completed for each target in both tasks. No other selection criteria have been applied. From the original population of 162 neurons, this procedure yielded 145 neurons for analysis (89 in monkey 1, M1, 56 in monkey 2, M2).

Single neuron activity was recorded and then quantified into spike counts calculated in 100ms bins that were then used to build up features population vectors to train the MLE and Naïve Bayes (NB) decoders. Thus a single features vector included, for a given time bin, spike counts calculated for each element (neuron) of the examined population, that is 89 elements for monkey 1 and 56 for monkey 2. Features space was obtained concatenating horizontally all 10 trials by 9 possible positions (90 feature vectors). Note that neurons were recorded one at time, therefore feature vectors describe the activity of a pseudo-population (2.3.1).

We were interested in studying to what extent signals extracted from V6A could support cognitive neuro prosthetics. Unlike the traditional approach where the trajectory of movement is decoded, here we used a combinations of MLE and NB decoders to decode: a) target location, b) the intention to perform a reach or a non-spatial motor response and c) the different phases that follow one another for the realization of the movement, free, delay and movement.

3.1 Target decoding. The first property we decoded was target position in space. We have previously decoded target position in categorical space (left/right, near/far) using a Bayesian classifier (42). Given that the space is a continuous physical quantity, such method would have insufficient application in real life conditions. To overcome this limitation, we employed here an MLE decoder which, starting from the *x, y* coordinates of target position in space (x,*y* for direction and depth axis, respectively) and the corresponding spike counts, fitted a polynomial regression surface for each neuron. Using Bayes' rule we calculated continuous maps which describe the probability of target's *x,y* location given a spike count. Combining maps across neurons we obtained the most likely target position given the population spike counts vector.

Figure 3 reports the results of this analysis performed on a time interval that spanned from 500ms before, till the movement onset for M1 and M2 populations. Averaged decoded positions (black dots) were typically very close to the real position of targets (green crosses). Estimated positions using signals from M1 population (n=89) yielded good accuracy and precision: we calculated an overall mean constant error (over 100 cross validations and 9 positions) of 1.1 cm (S.D. 1.1) and a mean dispersion of 1.4 cm (Fig.3 left, S.D. 1.2). For M2 population, we found similar results with a mean constant error of 0.9 cm (SD 0.6) and a mean dispersion of 2.3 cm (Fig.3 right, SD 2.1). Besides a lower accuracy for M2 monkey probably due to a smaller neural population, results were very comparable between the two monkeys. Similar results were obtained pooling together neurons from M1 and M2 (compare M1 results with Fig.4 where M1 + M2 population was used) with an even higher precision and accuracy, 1.1cm, SD 0.7, and 1.1cm, SD 0.8, respectively. The analyses presented below were obtained by pooling together data from M1 and M2.

First, we analyzed three distinct 300-ms intervals in each task (Fig. 1D). The first interval, termed 'early delay', extended from the beginning of target fixation till 300 ms after it. The second interval, 'late delay', included the last 300 ms before the 'Go" cue. While in 'early delay' visuospatial signals related to the newly fixated target were expected to be dominant, in the 'late delay' we assumed that activity would also be influenced by the preparation of the upcoming movement. The third interval we analyzed started at the 'GO' cue and lasted for 300 ms, thus encompassing monkey's reaction time, which is variable between trials (285 ms SD 44 ms), and part of movement (409 ms SD 99 ms from the release of the home button to the touch of the target). By examining these three intervals we examined whether decoding accuracy of target's location changes across distinct task stages.

Overall results of Figure 4 show a high decoding performance in all three intervals. Decoding accuracy increased moving toward the movement onset, with distances (ellipses size) between predicted and real target position progressively decreasing throughout the task. No remarkable differences were noticeable between the fix-reach and fix-lift tasks (Mann-Whitney test, $p>0.05$).

While using wide time intervals (i.e. 300 ms) for the analysis reduces noise increasing overall decoding performance, it provides less information about the dynamics of neural coding. To resolve this issue, we performed the same decoding analysis using a 100-ms window that moved in steps of 20 ms. A full 100-fold cross-validation was performed, R^2 values were plotted as function of time (Fig. 5). Blue and red solid lines of Figure 5 refer to R^2 values for cross-validated models of fix-reach and fix-lift tasks, respectively. Decoding accuracy started to increase as soon as the target was presented (Fig.1, LED ON), was stable during delay and movement and then decreased at the end of each task. This performance was used as reference for the generalization analysis. With this analysis we investigated how much the task-specific movements (reach vs hand lift) affected the population activity. Generalization typically works well in case of similar pattern of neural activity, whereas poor results are obtained when neural codes differ. The generalization analysis was implemented by training the MLE decoding algorithm on one task and testing it on the other task, with results plotted as dashed lines in Figure 5. As shown, the generalization performance during the delay epoch was comparable with decoding performed within the same task (solid lines), suggesting that activity during delay reflected mostly an abstract encoding of movement preparation and/or cue anticipation shared between the two tasks. Differently, after GO signal the generalization performance dropped abruptly. This finding most likely reflects the different motor response (reach vs. hand lift).

3.2. Task decoding. The generalization analysis reported in Figure 5 showed that the patterns of population activity in the two tasks were similar during the delay period and then they diverged immediately before and during the movement. The similarity during the delay makes questionable whether it is feasible to extract task-specific information from the activity before the movement execution. This information would be useful for a prosthesis about the real intention of the subject. To maximize the differences in neuronal activity linked to the specific movement plans of the two tasks and to allow a decoder to better discriminate between them, we performed another analysis. We used the residuals from regressions fits performed for the MLE decoding described above as feature to train a Naïve Bayes classifier. Residuals describe how much the observed data (spike counts) deviated from the model; in this case, polynomial fit was calculated pooling together the fix-reach and fix-lift datasets, thus plausibly the model was halfway between the real data of fix-reach and fix-lift, making the residuals suitable to describe the differences. As shown in Figure 6 the Naïve Bayes decoder correctly assigned, to fixate-to-reach or fixate-to-lift, residuals coming from the polynomial model. Recognition rates were above 90% before and after the GO signal, thus confirming the feasibility of extracting the task-specific motor plan well before movement onset.

3.3. State decoding. To develop neural prosthetics as autonomous as possible, the algorithm would have to determine when the subject intend to start the action. Decoding of neural states has been pursued as trigger for neuroprosthetic control (17,34). Yet identifying the exact temporal sequence of neural states can help to understand how similar neural activation patterns are reused in different tasks, and how these latent states gradually evolve towards movement execution (43). PPC seems to be the ideal region to extract information regarding task phases, as PPC neurons often exhibit activity modulation according to the task phase (24,29,44,45). To examine this aspect, we trained a Naive Bayes classifier to recognize the correct task phase between FREE, DELAY and MOV epochs given the spike counts in these epochs. We found that the high probabilities of a certain state matched the behavioral epoch that was source of spike counts. Accordingly, it was possible to identify the correct task state giving spike counts from a random 100 ms bin (Fig. 7A, top row) both for fix-reach and fix-lift. Applying the generalization approach (Fig. 7A, bottom row) yielded accurate epoch recognition during FREE and DELAY (i.e. the fix-reach and fix-lift codes are very similar). As expected, MOVEMENT epoch is not recognized in the context of generalization because of the very different nature of movement type between the tasks (reaching *vs* hand lift). Accuracy score for single classes (epochs) reported in confusion matrices (Fig.7B) are consistent with state probabilities of Fig.7A: codes are very similar during free and delay epoch, but not during MOV. For the MOV epoch, in particular where the decoder was trained during the fix-reach and tested during the fix-lift task, the classifier yielded a rather unexpected result. In fact, state probabilities were unbalanced towards being in the state delay (see green line in the corresponding box of Fig.7A), this lead to a bias in the confusion matrix where a 33% chance level was expected (here 83% of MOV bins were attributed to the delay epoch). The result indicates that during the movement epoch of the fix-lift task visuospatial information that is present also in fix-reach task is preserved. On the contrary, visuospatial signals in fix-lift task were not strong enough to support decoding generalization in the fix-reach task. In other words, while in the case of the fix-reach task the information about the spatial position of the target remained relevant during MOV, this was not the case for the corresponding interval of the fix-lift task where the simple release of the button did not require spatial information.

4. Discussion

We examined whether we could decode from the population activity of PPC area V6A information regarding the target position, the required movement type and the time interval along the task progress at the same time. We trained a MLE algorithm to yield a metric estimation of the target positions. Then we used a combination of MLE and a NB classifier to obtain a classification of task type. Finally, we demonstrated that, supplying the algorithm with spike counts from small time intervals of the trial, these were attributed correctly to the corresponding free, delay or movement epoch.

Taken together, these results indicate that neurons in V6A encode, in the same population, several types of information such as spatial position, intention for a specific motor response and progress of the task. This finding supports the idea that neurons are not simply tuned to a single feature, but they encode several task-relevant variables in the same time. Decoding of multiple parameters from the same area could be advantageous for BCI applications in terms of implant invasiveness and accuracy of the reconstructed information.

4.1 Decoding of visuospatial, movement planning and motor signals.

Monkeys performed both tasks while always looking at the targets, so our task cannot discriminate whether we are solely decoding gaze position or attentional/visuospatial signals useful to guide the motor response. In a previous work where we dissociated gaze from target, the decoding of target position was still possible, though less accurate (42). This suggested that V6A neurons carry both attentional and gaze signals. Signals related to gaze position and visuospatial attention have been shown to be useful for decoding and neuroprosthetic purposes (46–48). Thus, although in the present case it was not possible to separate the two components, this is not a limitation for the proposed method, since often the spatial attention matches the gaze position in naturalistic conditions.

Single cell analysis over the population used here showed that about 44% of cells were influenced by both target location and task type. Another fraction of cells (25%) were tuned by target location, but not task type, while a smaller number (17%) encoded task type only (33). Given the tight relationship between the tuning of a neural population to a given parameter and the decoding accuracy of that parameter using population activity(42,49–51), it should be taken for granted that each of the homogeneous sub-populations mentioned above would excel in decoding the variable(s) that is tuned for. For example, the sub-population of cells sensitive only to the type of task (i.e. their firing rate does not significantly change between different spatial position), will not contribute to the spatial position decoding of the target, which would rely on signals from the other two subpopulations. At this regard, the reliable decoding of target position from population signals in both tasks (Fig.5), is in line with the high incidence (44% + 25%) of neurons sensitive to target location as reported in Breveglieri et al.(32) and was also confirmed by the generalization analysis**.** Our decoding analyses put together these subpopulations in order to extract information from the whole population activity and thus achieve the best decoding performance.

Generalization of decoders between tasks can help to examine the nature of encoded information. Different authors used a generalization approach to test stationarity of temporal code within a neural population (51–53), or to compare population activation patterns between different, but related tasks (43). Similarly, we wanted to compare codes employed for tasks that shared initial stages, but differed in the subsequent motor response and its related planning. After the GO signal, the neural population activity changed to encode the upcoming movement, so the decoder's generalization performance dropped rather abruptly.

Slightly before the Go signal, the generalization performance was still high, thus suggesting that planning activity was similar between the two tasks. This finding, though surprising, might be attributed to the presence of a default reach plan/intention also when no reach is executed, as some evidence suggests (54,55). However, given that the two tasks were performed in separate blocks, the animal was always aware whether it was required to perform a reach movement, or simply lift its hand. Furthermore, given that a simple hand lift was enough to obtain the reward, we would expect that monkey's intention and commitment to perform a reach was significantly attenuated in the fixation-to-lift task. In line with this view, Breveglieri et al. (33) found that the majority of V6A cells show different activity between these two tasks. Whether these neurons were still encoding a default or uncompleted reach plan cannot be answered directly in the present study. Nevertheless, we could still discriminate task type (Fig.6) despite the fact that the codes were very similar during the delay (code generalization of Fig. 5). Such a result would not have been achieved if the neural codes in the two tasks were the same. The high levels of generalization obtained in the period before the movement could be attributed to the strong visuospatial signals in V6A that, being invariant between tasks, masked the task-specific signals related to movement planning and preparation.

Our decoding method was based on fitting residuals. Residuals represent the distance between actual spike counts and regression surfaces: thinking at these surfaces as a midline between fixate-to-reach and fixate-to-lift condition (because of fitting of dispersed data), shifts from this midline are still informative about the task type. A point of strength of this analysis is the type of feature we used in the classifier. The model was computed pooling together data from different target positions; this ensures that the present method works independently from position constraints. The possibility to discriminate in advance if the subject will execute the reach movement or just lift the hand, could be potentially useful for neuroprosthetic purposes. In case where a Go signal is spatially dissociated from the target of the action (e.g. clicking a computer mouse while looking at the screen), decoded information may allow to select the appropriate action: to prepare for moving or to withhold the robotic limb. In our case the decoding is limited to distinguish two scenarios, but the system could be trained to recognize different tasks and act accordingly.

4.2 Metric estimation of target position from PPC.

In a previous work we used a Bayesian classifier from PPC activity to discriminate between the nine target positions on the same panel used here (42). This method yielded very high target recognition rates and a small neuronal population was sufficient to obtain very good results (about 10-20 neurons). The present method enables a metric estimation of target positions at the cost of a larger number of neurons required to give an accurate prediction. 56 neurons were found to be barely enough (see very high dispersion in M2 case) to get a good decoding accuracy, whereas ~90 neurons (see M1 case) were fairly enough. Given that simple (second-order) polynomials were used to model single neuron tuning, our results suggest that good performance could also be observed for intermediate target positions never seen by the decoder. This is a desirable characteristic for a fully implemented neural decoder.

4.3 Encoding of task progress.

Thus, V6A signals were adequate to obtain a metric estimation of target, both in the fix-reach and fix-lift task, and to decode the intended action. In addition, we provided evidence that a time interval of 100 ms, putting together contributions of a population of V6A neurons, was sufficient to decode reliably the corresponding phase in the task progress (Fig.7A-B). Although much effort has been put into decoding intended reaching goals (2,16,56), deciphering the intended action onset is equally important (17,34,57). Different task phases have been typically correlated to different neural states, proceeding through the tasks entail moving through neural states. So, in our fix-reach task we expected at least three neural states: a resting state (no task engagement), a waiting time where the animal waited the go signal and finally the actual reaching movement. A similar task was studied in premotor areas (34). They used a hidden Markov model (HMM) to detect baseline, preparation and execution states. In addition, they implemented an extended model to decode multiple states, one for each reaching goal. In another study a four states (additional holding state) HMM was used to detect hidden neural states and so to develop a task independent decoder (58). Here we used a simpler, but equally informative, Bayesian decoder to obtain posterior probabilities of free, delay and movement states. Our results demonstrate that also signals from V6A are adequate to detect the switch from pre-movement to movement neural state that might be useful to trigger neural prosthesis movement.

4.4. Different parameters encoded in the same circuit is advantageous for BCI.

A large amount of evidence has already reported that single PPC neurons can encode both spatial (sensory) and non-spatial (cognitive) information (53,58–61). For example, attention toward a specific spatial location or toward non-spatial visual features modulate lateral intraparietal neurons (51,61,62), parietal reach region encodes both the target location and the movement intention (59,60). Information of spatial location of target and the intention for performing one action or another are of great interest for neuroprosthetic applications, yet few works tried to perform population decoding of both spatial and non-spatial PPC signals and explore the potential from a neuroprosthetic perspective. In Hauschild et al.(14), monkey brain activity controlled a cursor in a 3D environment, but the cognitive information that can be decoded from PPC to improve the decoder was not considered. Similarly another study by Shenoy and colleagues (17) decoded the information about task stage, either free, plan or movement, but they did not attempt to generalize the decoder over other tasks.

Recent studies have demonstrated that neurons in parietal (24,63–68) and frontal (69,70) areas have mixed selectivity: individual neurons are modulated by multiple task parameters. Rather than having specialized networks for specific behaviors, mixed selectivity is considered to offer a significant computational advantage by encoding multiple feature information over a single neural network (69,71,72). In everyday life, we often look at objects that we are going to reach and grasp, but we also look and attend to stimuli in one location and perform a motor response in another location. Here we provide evidence that both action plans that involve different sensory-to-motor transformations can be decoded from the same neural population in V6A and this finding is relevant also as fundamental knowledge.

4.5 Future application in human.

Functional MRI studies proposed a putative human homologue of area V6A (35), which approximately corresponds to the anterior part of the superior parieto-occipital cortex (SPOC) (12). SPOC shows enhanced visual activation to objects presented within the peripersonal space, even when the potential action is not actually executed (73). Decoding of pre-movement activity of SPOC with fMRI pattern analysis allowed reliable classification of specific actions that were subsequently performed, with a clear distinction between reaching and grasping movements (19). Although fMRI technique does not allow to study mixed selectivity due to poor spatial resolution, analogies between monkey and putative human V6A (35,74) give hope to translate findings from monkey to human.

5. Conclusions

In conclusion, these results show that V6A signals can be used to reliably decode visuospatial properties, information about the type of intended movement (spatial, goal-directed reach, or non-spatial button release), and task progression. Recently, V6A signals were used to decode up to 5 grip types during a grasping task and 9 different goal locations during reach (41,42). Previous and present results support prostheses that extract the target of a movement and respond as the intention to move is formed. Furthermore, present findings show that conditional motor responses like when a visual cue instructs a movement somewhere else in space could be also decoded and subsequently used to control a prosthesis. Having multiple information coded in a single area is advantageous for neuroprosthetics, allowing a single electrode array to decode multiple action scenarios.

Funding

This work was supported by European Union (H2020-MSCA-734227 – PLATYPUS), by Ministero dell'Università e della Ricerca (Italy, PRIN2017-2017KZNZLN), by Fondazione Cassa di Risparmio in Bologna, Bando Ricerca 2018/0373, by National Health and Medical Reasearch Council (Australia, NHMRC APP1083898, NHMRC APP1082144).

Acknowledgements

We thank Drs. Federica Bertozzi and Giulia Dal Bo' for help in the recordings, Massimo Verdosci and Francesco Campisi for technical assistance.

References

1. Hochberg LR, Bacher D, Jarosiewicz B, Masse NY, Simeral JD, Vogel J, et al. Reach and grasp by people with tetraplegia using a neurally controlled robotic arm. Nature. 2012;485(7398):372–5.
2. Aflalo T, Kellis S, Klaes C, Lee B, Shi Y, Pejsa K, et al. Neurophysiology. Decoding motor imagery from the posterior parietal cortex of a tetraplegic human. Science. 2015 May 22;348(6237):906–10.
3. Collinger JL, Wodlinger B, Downey JE, Wang W, Tyler-Kabara EC, Weber DJ, et al. High-performance neuroprosthetic control by an individual with tetraplegia. Lancet. 2013 Feb;381(9866):557–64.
4. Velliste M, Perel S, Spalding M, Whitford A, Schwartz A. Cortical control of a robotic arm for self-feeding. Nature. 2008;453(June):1098–101.
5. Carmena JM, Lebedev MA, Crist RE, O'Doherty JE, Santucci DM, Dimitrov DF, et al. Learning to control a brain-machine interface for reaching and grasping by primates. PLoS Biol. 2003;1(2):E42.
6. Wessberg J, Stambaugh CR, Kralik JD, Beck PD, Laubach M, Chapin JK, et al. Real-time prediction of hand trajectory by ensembles of cortical neurons in primates. Nature. 2000;408(6810):361–5.
7. Mountcastle VB, Lynch JC, Georgopoulos A, Sakata H, Acuna C. Posterior parietal association cortex of the monkey: command functions for operations within extrapersonal space. J Neurophysiol. 1975 Jul 1;38(4):871–908.
8. Andersen RA, Snyder LH, Bradley DC, Xing J. MULTIMODAL REPRESENTATION OF SPACE IN THE

POSTERIOR PARIETAL CORTEX AND ITS USE IN PLANNING MOVEMENTS. Annu Rev Neurosci. 1997;

9. Andersen RA, Burdick JW, Musallam S, Pesaran B, Cham JG. Cognitive neural prosthetics. Vol. 8, Trends in Cognitive Sciences. 2004. p. 486–93.
10. Kalaska JF, Scott SH, Cisek P, Sergio LE. Cortical control of reaching movements. Curr Opin Neurobiol. 1997 Dec;7(6):849–59.
11. Culham JC, Cavina-Pratesi C, Singhal A. The role of parietal cortex in visuomotor control: What have we learned from neuroimaging? Neuropsychologia. 2006 Jan;44(13):2668–84.
12. Gallivan JP, Culham JC. Neural coding within human brain areas involved in actions. Curr Opin Neurobiol. 2015 Aug;33:141–9.
13. Gallivan JP, Goodale MA. The dorsal “action” pathway. In: Handbook of clinical neurology. 2018. p. 449–66.
14. Hauschild M, Mulliken GH, Fineman I, Loeb GE, Andersen RA. Cognitive signals for brain-machine interfaces in posterior parietal cortex include continuous 3D trajectory commands. Proc Natl Acad Sci U S A. 2012 Oct;109(42):17075–80.
15. Mulliken GH, Musallam S, Andersen RA. Decoding trajectories from posterior parietal cortex ensembles. J Neurosci. 2008;28(48):12913–26.
16. Musallam S, Corneil BD, Greger B, Scherberger H, Andersen R. Cognitive control signals for neural prosthetics. Science. 2004;305(5681):258–62.
17. Shenoy K V., Kureshi SA, Pesaran B, Buneo CA, Andersen RA, Meeker D, et al. Neural prosthetic control signals from plan activity. Neuroreport. 2003 Mar 24;14(4):591–6.
18. Gertz H, Lingnau A, Fiehler K. Decoding Movement Goals from the Fronto-Parietal Reach Network. Front Hum Neurosci. 2017 Feb 24;11.
19. Gallivan JP, McLean DA, Valyear KF, Pettypiece CE, Culham JC. Decoding action intentions from preparatory brain activity in human parieto-frontal networks. J Neurosci. 2011 Jun 29;31(26):9599–610.
20. Andersen RA, Cui H. Intention, Action Planning, and Decision Making in Parietal-Frontal Circuits. Neuron. 2009 Sep;63(5):568–83.
21. Hadjidimitrakis K, Bakola S, Wong YT, Hagan MA. Mixed Spatial and Movement Representations in the Primate Posterior Parietal Cortex. Front Neural Circuits. 2019 Mar 11;13:15.
22. Galletti C, Fattori P, Kutz DF, Gamberini M. Brain location and visual topography of cortical area V6A in the macaque monkey. Eur J Neurosci. 1999 Feb;11(2):575–82.
23. Galletti C, Kutz DF, Gamberini M, Breveglieri R, Fattori P. Role of the medial parieto-occipital cortex in the control of reaching and grasping movements. In: Experimental brain research. 2003. p. 158–70.
24. Hadjidimitrakis K, Bertozzi F, Breveglieri R, Bosco A, Galletti C, Fattori P. Common neural substrate for processing depth and direction signals for reaching in the monkey medial posterior parietal cortex. Cereb Cortex. 2014;24(6):1645–57.
25. Fattori P, Raos V, Breveglieri R, Bosco A, Marzocchi N, Galletti C. The dorsomedial pathway is not just for reaching: grasping neurons in the medial parieto-occipital cortex of the macaque monkey. J Neurosci. 2010;30(1):342–9.
26. Fattori P, Breveglieri R, Bosco A, Gamberini M, Galletti C. Vision for Prehension in the Medial Parietal Cortex. Cereb Cortex. 2017 Dec 1;27(2):1149–63.
27. Hadjidimitrakis K, Breveglieri R, Bosco A, Fattori P. Three-dimensional eye position signals shape both peripersonal space and arm movement activity in the medial posterior parietal cortex. Front Integr Neurosci. 2012;6:37.
28. Fattori P, Gamberini M, Kutz DF, Galletti C. “Arm-reaching” neurons in the parietal area V6A of the macaque monkey. Eur J Neurosci. 2001 Jun;13(12):2309–13.
29. Fattori P, Kutz DF, Breveglieri R, Marzocchi N, Galletti C. Spatial tuning of reaching activity in the medial parieto-occipital cortex (area V6A) of macaque monkey. Eur J Neurosci. 2005 Aug;22(4):956–72.
30. Hadjidimitrakis K, Breveglieri R, Placenti G, Bosco A, Sabatini SP, Fattori P. Fix your eyes in the space you could reach: neurons in the macaque medial parietal cortex prefer gaze positions in

peripersonal space. Gribble PL, editor. PLoS One. 2011 Aug 17;6(8):e23335.
31. Breveglieri R, Hadjidimitrakis K, Bosco A, Sabatini SP, Galletti C, Fattori P. Eye position encoding in three-dimensional space: integration of version and vergence signals in the medial posterior parietal cortex. J Neurosci. 2012 Jan 4;32(1):159–69.
32. Hadjidimitrakis K, Ghodrati M, Breveglieri R, Rosa MGP, Fattori P. Neural coding of action in three dimensions: Task- and time-invariant reference frames for visuospatial and motor-related activity in parietal area V6A. J Comp Neurol. 2020;
33. Breveglieri R, Galletti C, Dal Bò G, Hadjidimitrakis K, Fattori P. Multiple aspects of neural activity during reaching preparation in the medial posterior parietal area V6A. J Cogn Neurosci. 2014 Apr;26(4):878–95.
34. Kemere C, Santhanam G, Yu BM, Afshar A, Ryu SI, Meng TH, et al. Detecting Neural-State Transitions Using Hidden Markov Models for Motor Cortical Prostheses. J Neurophysiol. 2008;100(4):2441–52.
35. Pitzalis S, Sereno MI, Committeri G, Fattori P, Galati G, Tosoni A, et al. The human homologue of macaque area V6A. Neuroimage. 2013 Nov 15;82:517–30.
36. Galletti C, Fattori P, Gamberini M, Kutz DF. The cortical visual area V6: brain location and visual topography. Eur J Neurosci. 1999 Nov;11(11):3922–36.
37. Morris AP, Krekelberg B. A Stable Visual World in Primate Primary Visual Cortex. Curr Biol. 2019 May 6;29(9):1471-1480.e6.
38. Morris AP, Bremmer F, Krekelberg B. Eye-position signals in the dorsal visual system are accurate and precise on short timescales. J Neurosci. 2013 Jul 24;33(30):12395–406.
39. Morris AP, Kubischik M, Hoffmann K-P, Krekelberg B, Bremmer F. Dynamics of Eye-Position Signals in the Dorsal Visual System. Curr Biol. 2012 Feb 7;22(3):173–9.
40. Morris AP, Bremmer F, Krekelberg B. The Dorsal Visual System Predicts Future and Remembers Past Eye Position. Front Syst Neurosci. 2016 Feb 24;10:9.
41. Filippini M, Breveglieri R, Akhras MA, Bosco A, Chinellato E, Fattori P. Decoding Information for Grasping from the Macaque Dorsomedial Visual Stream. J Neurosci. 2017 Apr;37(16):4311–22.
42. Filippini M, Breveglieri R, Hadjidimitrakis K, Bosco A, Fattori P. Prediction of Reach Goals in Depth and Direction from the Parietal Cortex. Cell Rep. 2018;23(3):725–32.
43. Mazurek KA, Rouse AG, Schieber MH. Mirror Neuron Populations Represent Sequences of Behavioral Epochs During Both Execution and Observation. J Neurosci. 2018 May 2;38(18):4441–55.
44. Cui H, Andersen RA. Posterior Parietal Cortex Encodes Autonomously Selected Motor Plans. Neuron. 2007;56(3):552–9.
45. Stetson C, Andersen RA. Early planning activity in frontal and parietal cortex in a simplified task. J Neurophysiol. 2015 Jun;113(10):3915–22.
46. Astrand E, Wardak C, Ben Hamed S. Selective visual attention to drive cognitive brain machine interfaces: from concepts to neurofeedback and rehabilitation applications. Front Syst Neurosci. 2014 Aug 12;8.
47. Andersen RA, Hwang EJ, Mulliken GH. Cognitive neural prosthetics. Annu Rev Psychol. 2010 Jan;61:169–90, C1-3.
48. Batista AP, Yu BM, Santhanam G, Ryu SI, Afshar A, Shenoy KV. Cortical Neural Prosthesis Performance Improves When Eye Position Is Monitored. IEEE Trans Neural Syst Rehabil Eng. 2008 Feb;16(1):24–31.
49. Bremmer F, Kaminiarz A, Klingenhoefer S, Churan J. Decoding target distance and saccade amplitude from population activity in the macaque lateral intraparietal area (LIP). Front Integr Neurosci. 2016;
50. Lehmann SJ, Scherberger H. Reach and gaze representations in macaque parietal and premotor grasp areas. J Neurosci. 2013 Apr 17;33(16):7038–49.
51. Astrand E, Ibos G, Duhamel J-R, Ben Hamed S. Differential Dynamics of Spatial Attention, Position, and Color Coding within the Parietofrontal Network. J Neurosci. 2015 Feb 18;35(7):3174–89.
52. Crowe DA, Averbeck BB, Chafee M V. Rapid Sequences of Population Activity Patterns Dynamically Encode Task-Critical Spatial Information in Parietal Cortex. J Neurosci. 2010 Sep 1;30(35):11640–53.
53. Meyers EM, Freedman DJ, Kreiman G, Miller EK, Poggio T. Dynamic Population Coding of Category Information in Inferior Temporal and Prefrontal Cortex. J Neurophysiol. 2008 Sep;100(3):1407–19.

54. Suminski AJ, Tkach DC, Hatsopoulos NG. Exploiting multiple sensory modalities in brain-machine interfaces. Neural Networks. 2009 Nov;22(9):1224–34.
55. Bremner LR, Andersen RA. Temporal Analysis of Reference Frames in Parietal Cortex Area 5d during Reach Planning. J Neurosci. 2014 Apr 9;34(15):5273–84.
56. Shanechi MM, Williams ZM, Wornell GW, Hu RC, Powers M, Brown EN. A Real-Time Brain-Machine Interface Combining Motor Target and Trajectory Intent Using an Optimal Feedback Control Design. Zhan W, editor. PLoS One. 2013 Apr 10;8(4):e59049.
57. Kao JC, Nuyujukian P, Ryu SI, Shenoy K V. A High-Performance Neural Prosthesis Incorporating Discrete State Selection with Hidden Markov Models. IEEE Trans Biomed Eng. 2017;
58. Sumsky SL, Schieber MH, Thakor N V., Sarma S V., Santaniello S. Decoding kinematics using task-independent movement-phase-specific encoding models. IEEE Trans Neural Syst Rehabil Eng. 2017;
59. Andersen RA, Buneo CA. Intentional Maps in Posterior Parietal Cortex. Annu Rev Neurosci. 2002;
60. Snyder LH, Batista a P, Andersen R a. Coding of intention in the posterior parietal cortex. Vol. 386, Nature. 1997. p. 167–70.
61. Bisley JW, Goldberg ME. Attention, Intention, and Priority in the Parietal Lobe. Annu Rev Neurosci. 2010 Jun;33(1):1–21.
62. Ibos G, Freedman DJ. Interaction between Spatial and Feature Attention in Posterior Parietal Cortex. Neuron. 2016 Aug 17;91(4):931–43.
63. Rishel CA, Huang G, Freedman DJ. Independent Category and Spatial Encoding in Parietal Cortex. Neuron. 2013 Mar;77(5):969–79.
64. Meister MLR, Hennig JA, Huk AC. Signal Multiplexing and Single-Neuron Computations in Lateral Intraparietal Area During Decision-Making. J Neurosci. 2013;
65. Park IM, Meister MLR, Huk AC, Pillow JW. Encoding and decoding in parietal cortex during sensorimotor decision-making. Nat Neurosci. 2014 Oct 31;17(10):1395–403.
66. Hadjidimitrakis K, Bertozzi F, Breveglieri R, Galletti C, Fattori P. Temporal stability of reference frames in monkey area V6A during a reaching task in 3D space. Brain Struct Funct. 2017 May 1;222(4):1959–70.
67. Bosco A, Breveglieri R, Hadjidimitrakis K, Galletti C, Fattori P. Reference frames for reaching when decoupling eye and target position in depth and direction. Sci Rep. 2016 Apr 15;6(1):21646.
68. Bosco A, Breveglieri R, Filippini M, Galletti C, Fattori P. Reduced neural representation of arm/hand actions in the medial posterior parietal cortex. Sci Rep. 2019 Dec 30;9(1):936.
69. Rigotti M, Barak O, Warden MR, Wang X-J, Daw ND, Miller EK, et al. The importance of mixed selectivity in complex cognitive tasks. Nature. 2013 May 19;497(7451):585–90.
70. Mante V, Sussillo D, Shenoy K V., Newsome WT. Context-dependent computation by recurrent dynamics in prefrontal cortex. Nature. 2013 Nov 6;503(7474):78–84.
71. Fusi S, Miller EK, Rigotti M. Why neurons mix: high dimensionality for higher cognition. Curr Opin Neurobiol. 2016 Apr;37:66–74.
72. Zhang CY, Aflalo T, Revechkis B, Rosario ER, Ouellette D, Pouratian N, et al. Partially Mixed Selectivity in Human Posterior Parietal Association Cortex. Neuron. 2017;
73. Gallivan JP, McLean A, Culham JC. Neuroimaging reveals enhanced activation in a reach-selective brain area for objects located within participants' typical hand workspaces. Neuropsychologia. 2011 Nov;49(13):3710–21.
74. Tosoni A, Pitzalis S, Committeri G, Fattori P, Galletti C, Galati G. Resting-state connectivity and functional specialization in human medial parieto-occipital cortex. Brain Struct Funct. 2015 Nov;220(6):3307–21.

Figures:

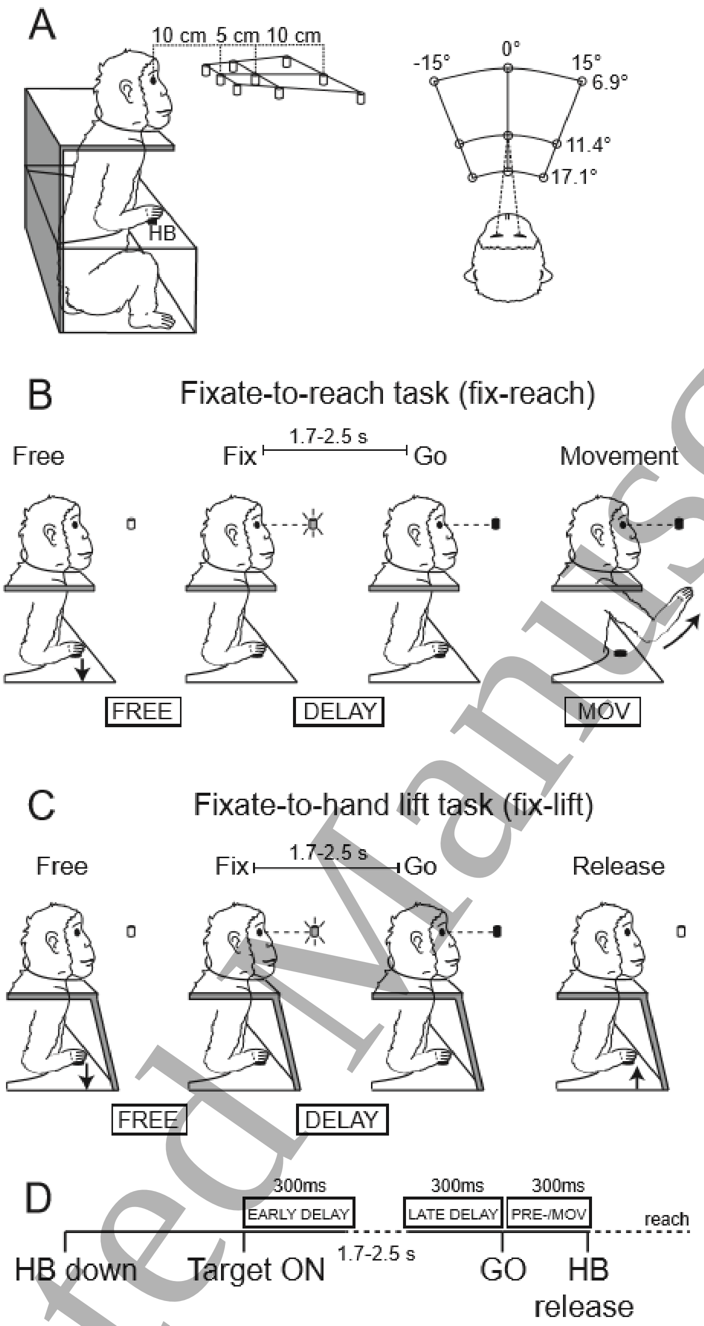

Figure 1. Experimental setup and schematic representation of the tasks. (A) Scheme of the setup used for the fix-reach and fix-lift tasks. Exact distances are indicated in the lateral (left) and top (right) views. Nine LEDs are used as targets, embedded in a panel located at eye level. HB = home button. (B, C) Time courses and behavioral epochs in the fix-reach (B) and fix-lift (C) tasks. The two tasks shared the first part, holding of home button, start of fixation, waiting for the GO signal. Then, in the fix-reach task the reaching movement is performed cued by the GO signal (target color changed from green to red), whereas in the fix-lift task the GO signal was the cue to lift the hand from the home button, and no reaching movement was performed. Black arrows indicate hand actions performed in the two tasks. (D) Schematic of the time intervals used in the analysis, with every interval lasting 300 ms. EARLY DELAY, from the start of the target fixation till 300 ms after it; LATE DELAY, the last 300 ms before the GO signal; PRE-/MOV, from the GO signal to 300 ms after it, this encompassed the reaction time plus the very first part of movement.

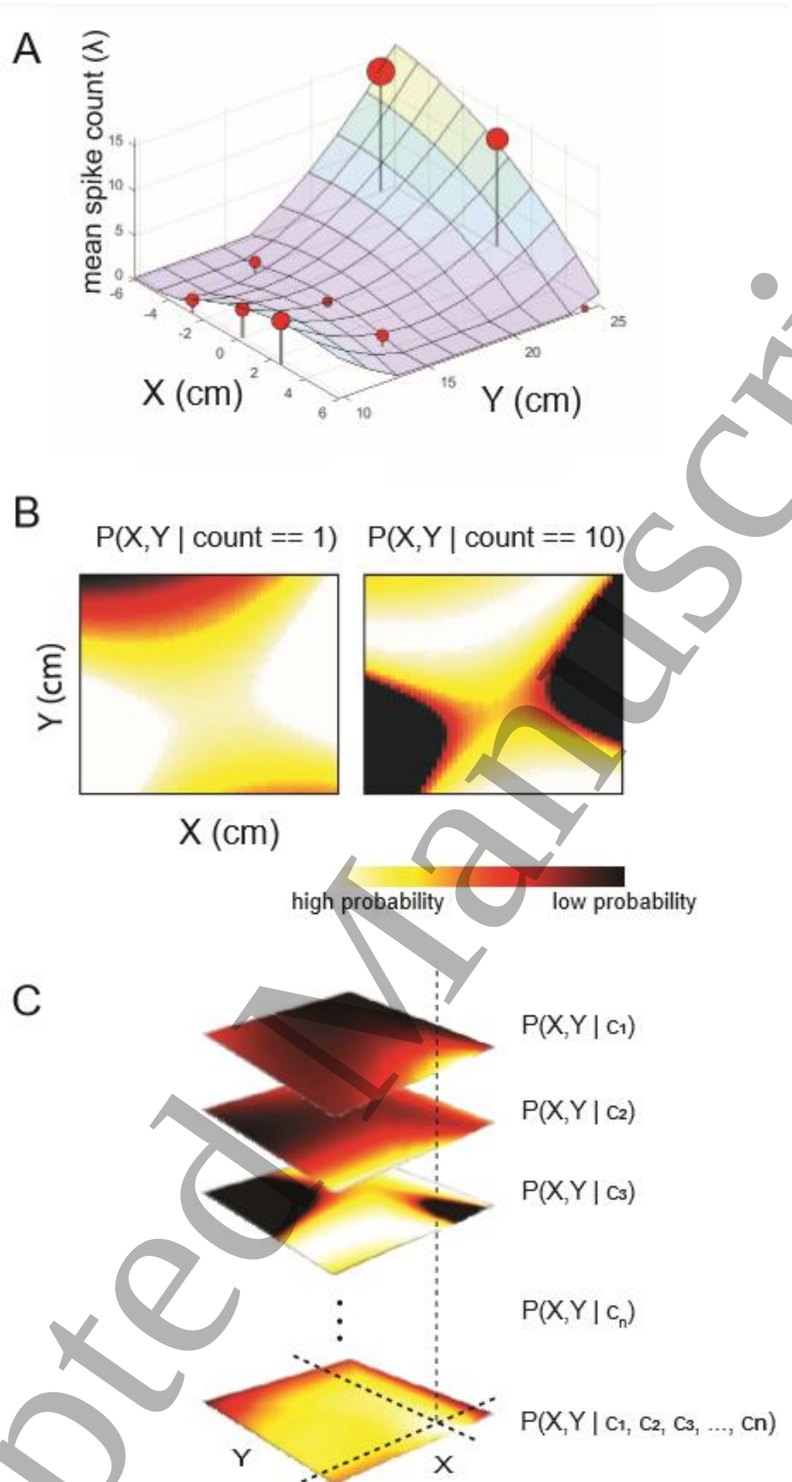

Figure 2. MLE decoder. (A) Activity of an exemplary V6A neuron and regression surface. In a first step a GLM was used to fit a regression surface over spike counts in the training set. Black vertical solid lines depict mean spike counts over the 9 panel positions with their standard deviation (red spheres). This neuron discharged for far positions, especially for the far-left position and was downregulated for intermediate positions. The regression surface was interpreted probabilistically, such that it specified the conditional probability of spike count given *x,y* target positions (*p(count | X,Y)*), assuming spike counts were Poisson-distributed. Using Bayes' rule, this could be converted to the probability of all target positions, X,Y, given a spike count *(p(X,Y | count)* in the test set. In (B) left, the probability map of neuron (A) given a low spike count (high probability in intermediate area) and (B) right, the probability maps given ahigh spike count (high probability for far and near area). (C) Given a vector of spike counts (c) for all neurons in a sample, (c1,c2, ..., cn), and corresponding probability maps, a population probability map was obtained by

summing the (log) probabilities. As the final step, the target position associated with the maximum a posteriori (MAP) log-likelihood (i.e., the MAP estimate) in log *p(X,Y | CountPopulation)* was selected as the point estimate.

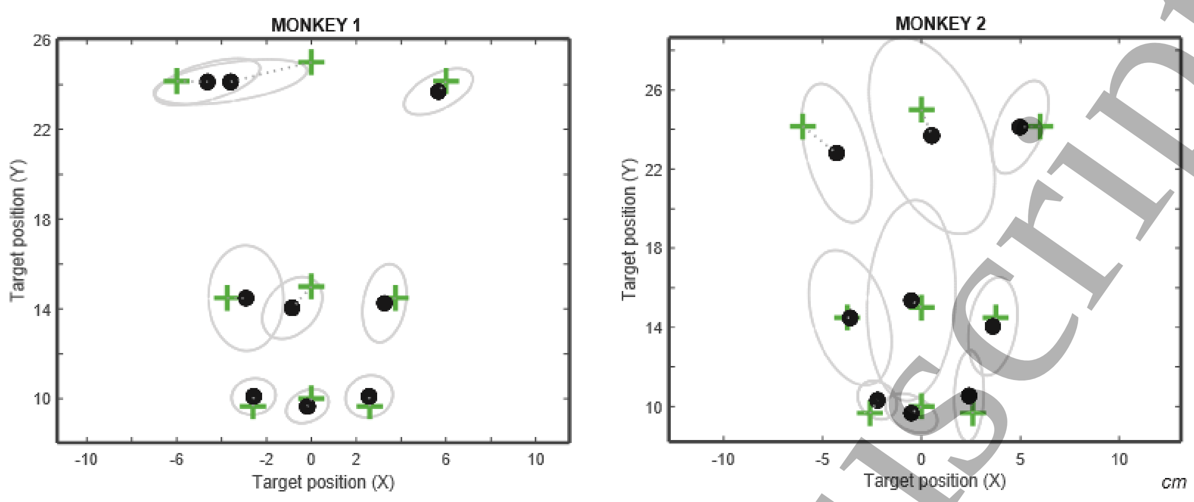

Figure 3. Metric estimation of target positions. The array of the 9 targets is illustrated in a two-dimensional view from above, green crosses show the real position of each targets, black dots are target estimated positions with their error distribution (light grey ellipses). Distances are reported in cartesian x,y (cm) coordinates, with x being the distance from the monkey's midsagittal level and y being the distance from the frontal eye level. Left panel, monkey 1 (89 neurons), right panel monkey 2 (56 neurons). Time analyzed was an interval of 500 ms before movement onset.

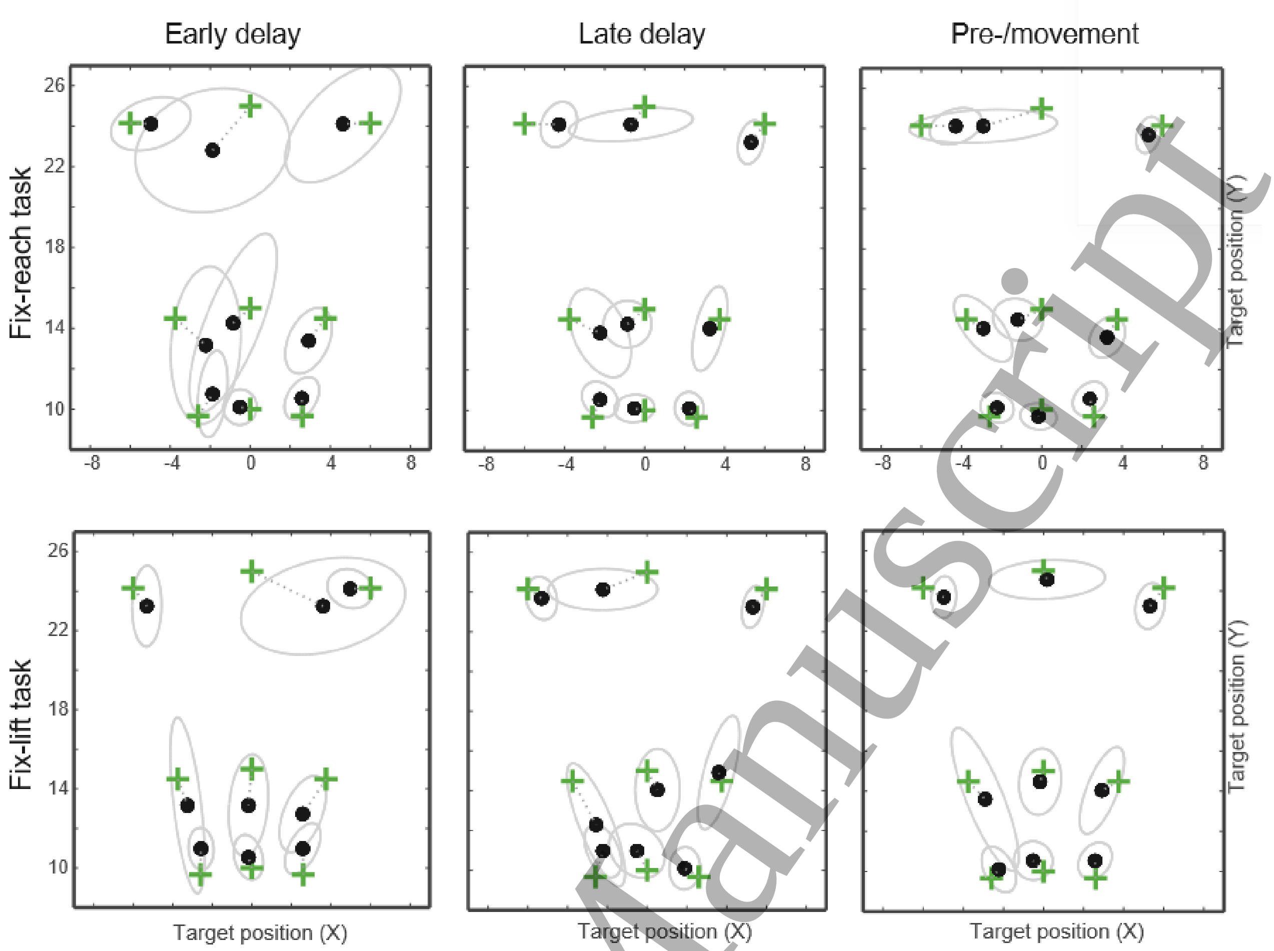

Figure 4. Metric estimation of targets position for different time intervals and tasks. Analysis was performed extracting spike counts from 100 ms time intervals and pooled together in 300 ms time windows corresponding to EARLY DELAY, LATE DELAY and PRE-/MOV epochs. These time intervals were analyzed for fix-reach task (top) where target position signals were transformed into arm action, and fix-lift task where no reaching movement was required (bottom). Neural population used in the analysis included both neurons from monkey 1 and monkey 2. Other conventions same as Figure 3.

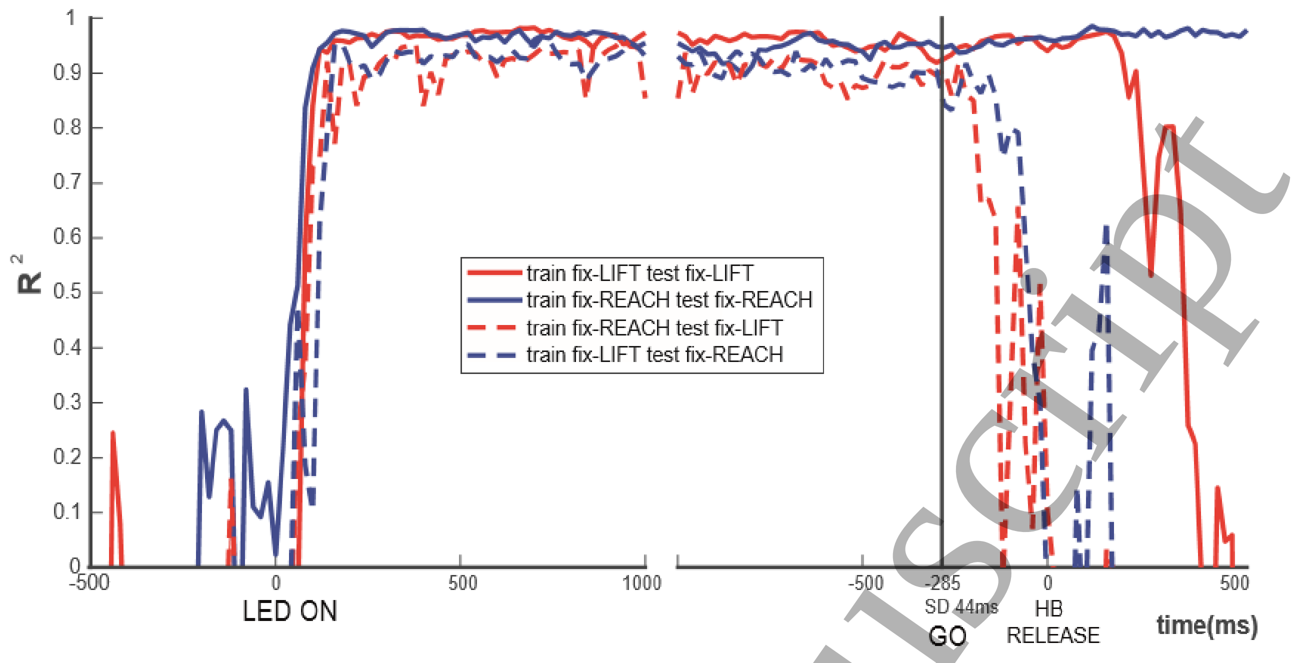

Figure 5. Decoding time course. R^2 values are reported for each of 100ms time intervals analyzed. The time window slid over the trial time with a 20ms step. Cross validated results are reported for fix-lift (solid red line) and fix-reach (solid blue line) tasks. A code generalization approach was used to obtain target estimations using the decoder trained with the opposite task dataset, that is, the algorithm was trained on fix-lift task and the code was generalized to decode fix-reach neural activity (blue dashed line), as opposed to training on fix-reach and estimation on fix-lift task (red dashed line). The plot required a double alignment (target LED ON and HB RELEASE, i.e. movement onset), as delay was randomized between trials. During the initial fixation and delay epochs across-task decoder performance was comparable to its within-task performance. This suggests that visuospatial and motor preparation codes were similar during the delay period. The two codes diverged shortly after the cue to execute the required motor response (reach/hand lift).

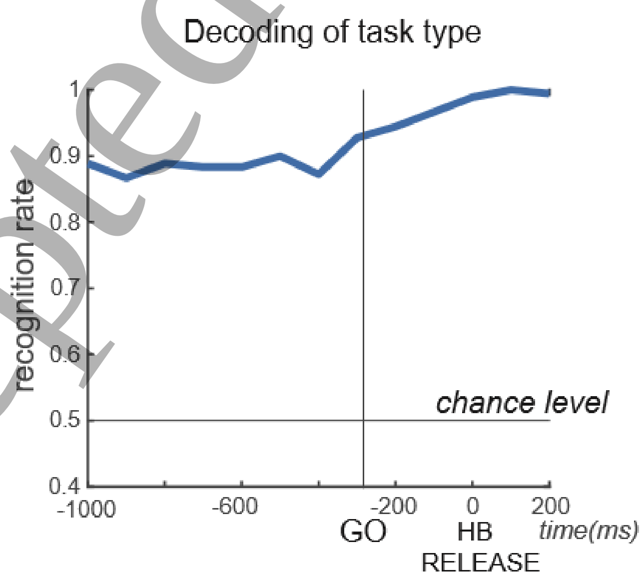

Figure 6. Decoding of task type. Binary classification of task type obtained feeding a naïve Bayes classifier with residuals from polynomial fits. Data from different targets were pooled together. A 50 folds' cross

validation was used. Residuals were good predictors for task type discriminations as evidenced by the recognition rate being always well above chance levels.

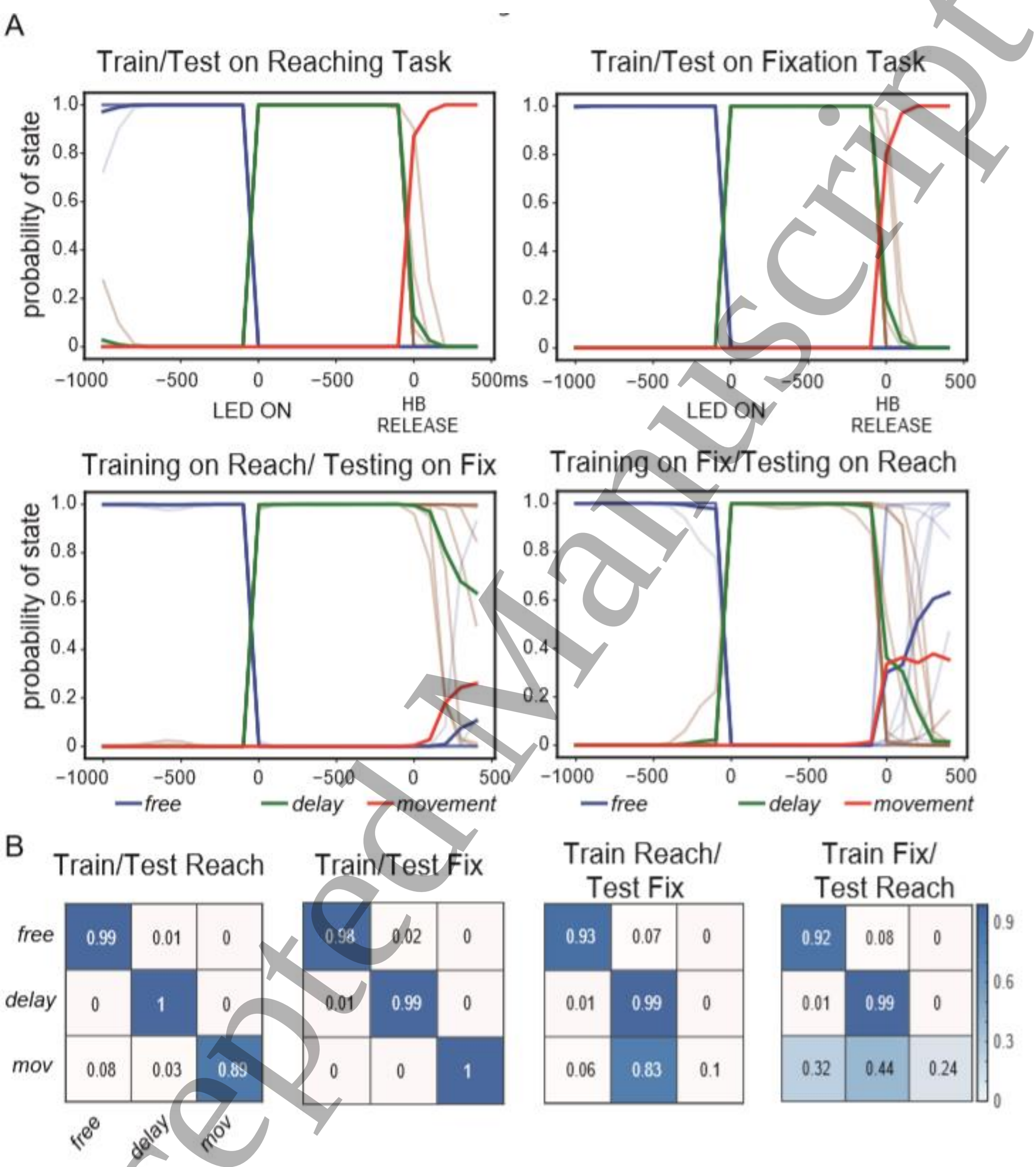

Figure 7. Decoding of task state. Spike counts were used as predictor of different task phases, free, delay or movement epochs. (A) Probability of each state, blue, green or red, respectively free, delay and movement states, were plotted over the time. Solid bold lines correspond to averages calculated over single trial probabilities (light lines). Due to different durations of delay between trials, two separate time intervals were artificially merged: 1 second before target led on (free epoch) and from -1.5s to 0.5s centered on movement onset. On the top row within-task decoding for reaching (left) and fixation (right) task are

shown, “leave one out” cross validation was used. Bottom row reports task generalization performance, i.e. training on fix-reach and testing on fix-lift task (left), and vice versa (right). During free and delay epochs the decoder can generalize across tasks; this gives an accurate epoch recognition, whereas movement epoch is correctly recognized only in the context of the same task**.** (B) The probabilities obtained for the states in Figure 7A were processed with an argmax function in order to calculate the classification results plotted in confusion matrices. The rows correspond to the real labels (epochs free, delay and movement), the columns to predicted labels.